The Amphibian Antimicrobial Peptide Uperin 3.5 is a Cross-α/Cross-β Chameleon Functional Amyloid

Nir Salinas[1,2‡], Einav Tayeb-Fligelman[1,3‡], Massimo Sammito[,4,5], Daniel Bloch[6], Raz Jelinek[6,7], Dror Noy[8], Isabel Uson[4,9], and Meytal Landau[1,10*]

[1]Department of Biology, Technion - Israel Institute of Technology, Haifa 3200003, Israel

[2]Present affiliation: Cardiovascular Research Institute, University of California San Francisco, San Francisco, CA 94158, USA

[3]Present affiliation: Chemistry and Biochemistry, UCLA DOE Institute of Genomics and Proteomics, University of California, Los Angeles 90095, USA

[4]Crystallographic Methods, Institute of Molecular Biology of Barcelona-Spanish Research Council (IBMB-CSIC), Barcelona Science Park, Baldiri Reixach 13-15, 08028 Barcelona, Spain

[5]Present affiliation: Department of Haematology, Cambridge Institute for Medical Research, University of Cambridge, Hills Road, Cambridge CB2 0XY, England

[6]Department of Chemistry, and [7]Ilse Katz Institute for Nanotechnology, Ben Gurion University of the Negev, Beer Sheva 84105, Israel

[8]Migal-Galilee Research Institute, Kiryat Shmona, Israel

[9]ICREA, Institució Catalana de Recerca i Estudis Avançats; Passeig Lluís Companys, 23; E-08003 Barcelona, Spain

[10]Centre for Structural Systems Biology (CSSB), and European Molecular Biology Laboratory (EMBL), Hamburg 22607, Germany

‡ These authors contributed equally

*Correspondence to: mlandau@technion.ac.il

Abstract

Antimicrobial activity is being increasingly linked to amyloid fibril formation, suggesting physiological roles for some human amyloids, which have historically been viewed as strictly pathological agents. This work reports on formation of functional cross-α amyloid fibrils of the amphibian antimicrobial peptide uperin 3.5 at atomic-resolution, an architecture initially discovered in the bacterial PSMα3 cytotoxin. The fibrils of uperin 3.5 and PSMα3 were comprised of anti-parallel and parallel helical sheets, respectively, recapitulating properties of β-sheets. Uperin 3.5 demonstrated chameleon properties of a secondary structure switch, forming mostly cross-β fibrils in the absence of lipids. Uperin 3.5 helical fibril formation was largely induced by, and formed on, bacterial cells or membrane mimetics, and led to membrane damage and cell death. These findings suggest a regulation mechanism, which includes storage of inactive peptides as well as environmentally induced activation of uperin 3.5, via chameleon cross-α/β amyloid fibrils.

Significance Statement

Salinas *et. al.* determined the crystal structure of the full-length amphibian antimicrobial peptide (AMP) uperin 3.5 and showed fibrillation into helical 'cross-α' amyloid fibril, correlated with its antibacterial activity. This provides a molecular basis for the link between AMPs which

are largely helical in nature, and amyloid formation. Uperin 3.5 is the first cross-α amyloid discovered in eukaryotes, following a previously reported cross-α amyloid fibril for *Staphylococcus aureus* PSMα3 cytotoxin, hence demonstrating the existence of the cross-α amyloid architecture across kingdoms of life, with potential functional roles in early evolution. Furthermore, the findings revealed a chameleon cross-α/cross-β secondary structure switch of uperin 3.5 fibrils, likely related to regulation of its activity.

Introduction

Antimicrobial peptides (AMPs) are found in all kingdoms of life, serving roles in the host-defense system by fighting microbial infections and killing cancerous cells(1-4). AMPs mainly target and disrupt membranes, leading to cell death (1), and, in some cases, their self-assembly into supramolecular structures enhances antimicrobial activity (5). Specifically, certain AMPs, such as dermaseptin S9, assemble into well-ordered fibrils that resemble amyloids, proteins which form a cross-β architecture comprised of tightly mated β-sheets (6-17). Human amyloids have primarily been associated with neurodegenerative and systemic diseases (18, 19), and evidence of antimicrobial properties for some, including the Alzheimer's associated amyloid-β and Parkinson's associated α-synuclein, suggest a physiological role in fighting infections threatening the brain (6, 20-26).

Our earlier investigations of functional amyloids revealed a distinct structure-function correlation in the phenol-soluble modulins (PSMs) family of peptides secreted by the *Staphylococcus aureus* bacterium, which are involved in virulence activities (27, 28), and form amyloid fibrils with specific morphologies (29-31). Specifically, the biofilm-associated PSMα1

and PSMα4 adopt the amyloid ultra-stable cross-β architecture (29), likely to serve as a scaffold rendering the biofilm a more resistant barrier. Exceptionally, PSMα3, which plays roles in cytotoxicity against human immune cells (27, 32), forms cross-α amyloid fibrils that are composed entirely of amphipathic α-helices. The helices stack perpendicular to the fibril axis into mated 'sheets' (31), just as the β-strands assemble in amyloid cross-β fibrils. Furthermore, a short segment from PSMα3 forms atypical β-rich fibrils with antiparallel orientation and shows a mild antibacterial activity (29). Overall, PSMαs show diverse activities as well as different morphologies of amyloid and amyloid-like fibrils. We previously showed that the ability of PSMα3 to form cross-α fibrils is critical for cytotoxicity, likely mediated through a dynamic process of co-aggregation with membrane lipids (31). Co-aggregation of amyloids with membrane lipids was previously suggested, for example for α-synuclein (33). Recently, various synthetic peptides, unnatural enantiomers and protein-mimics have been shown to form an architecture resembling cross-α (34-38).

Previous studies by Bowie, Carver, Martin and co-workers showed that the AMP uperin 3.5, secreted on the skin of *Uperoleia mjobergii* (Australian toadlet) (39), forms amyloid fibrils, and suggested an interaction with bacterial membrane lipids that stabilize its α-helical conformation (40-43). Moreover, by using uperin 3.5 mutants, they showed that a high α-helical content and lower net charge contribute to higher aggregation rate of the peptide (41, 42). Here, we demonstrate, at atomic resolution, that uperin 3.5 formed cross-α fibrils, which we suggest being essential for its toxic activity against the Gram-positive bacterium *Micrococcus luteus*. Moreover, the presence of bacterial membrane lipids induced a structural transition of uperin 3.5 into helical species in solution and in the fibrils, whereas their absence revealed a

chameleon behavior of a secondary structure switch into cross-β fibrils, which correlated with reduced antibacterial activity.

Results

Uperin 3.5 is a functional cross-α amyloid

The antimicrobial peptide uperin 3.5 self-assembled to form elongated amyloid fibrils, as visualized using transmission electron-microscopy (TEM), which bound the amyloid indicator dye thioflavin-T (ThT) (SI Appendix, Figure S1), similar to previous reports (40). The crystal structure of the full-length, 17-residue AMP, uperin 3.5, determined at 1.45 Å resolution (Table 1) (PDB code: 6GS3), revealed a cross-α fibril architecture (Figure 1). The cross-α fibrils of uperin 3.5 formed from stacks of amphipathic α-helices, positioned perpendicular to the fibril axis, creating a unique arrangement of mated 'helical sheets' extending along the fibril axis, similar to the β-sheets which form cross-β amyloid fibril architecture (6-17). Overall, the cross-α fibrils reassemble cross-β fibrils in their quaternary structures and in the ability to induce ThT fluorescence.

While the antibacterial amphibian uperin 3.5 and the cytotoxic bacterial PSMα3 showed low sequence similarity (SI Appendix, Figure S2A), both contained amphipathic helices and assembled into helical sheets that mate via a hydrophobic core (SI Appendix, Table S1 and visualized for uperin 3.5 in SI Appendix, Figure S2). However, while the PSMα3 helices are orientated in a parallel fashion (30), uperin 3.5 helices were arranged in an antiparallel manner (Figure 1). Thus, the cross-α amyloid fibril architecture can be encompassed by either parallel or antiparallel helical sheets. Uperin 3.5, in comparison to PSMα3, showed shorter inter-sheet and inter-helix distances, likely due to less bulky side chains (Figure 1). The high-order crystal packing of uperin 3.5 showed alternating hydrophobic and hydrophilic interfaces between rows

of sheets (SI Appendix, Figure S3), as seen in PSMα3 (30). The solvent-accessible surface area buried within the mated sheets of the cross-α uperin 3.5 fibril resembled that of PSMα3 (SI Appendix, Table S1), despite the shorter sequence of uperin 3.5. Nevertheless, the shape complementarity between the uperin 3.5 mated sheets was smaller than that of mated PSMα3 sheets (SI Appendix, Table S1), which might be related to the staggered orientation of the sheets (Figure 1). The staggered orientation might be compensated by higher-order packing in the fibril, with more than one pair of sheets per row (SI Appendix, Figure S3). Overall, the eukaryotic uperin 3.5 and the bacterial PSMα3 share a cross-α architecture but display extensive polymorphism in helix orientation and stacking.

In addition to the extensive hydrophobic core between sheets along the fibril, uperin 3.5 was also stabilized via an array of inter-helical polar bonds that ran along each sheet. These included inter-helical electrostatic interactions between Asp4 and Lys14, and an inter-helical hydrogen bond between the side chain of Arg7 and the amide carbonyl of Arg7 from an adjacent helix (SI Appendix, Figure S2D). Overall, each helix is potentially involved in four polar interactions along the sheet of stacked helices forming the cross-α fibril. Previous studies have indicated the importance of Arg7 in lipid interactions (41, 42), which aligns with our hypothesis, discussed below, that membrane interactions and the formation of cross-α fibrils are correlated processes.

Uperin 3.5 shows a chameleon propensity of a secondary structure switch in the presence of bacterial membrane lipids

In solution, uperin 3.5 formed a random-coil structure with typical minima at 197 nm, as measured using circular dichroism (CD) spectroscopy. This was in contrast to PSMα3, which is helical in solution(31). Nevertheless, the addition of small unilamellar vesicles (SUVs) composed

of 1,2-dioleoyl-sn-glycero-3-phosphoethanolamine (DOPE) and 1,2-dioleoyl-sn-glycero-3-phospho-(1'-rac-glycerol) (DOPG) at a 1:1 molar ratio, mimicking a Gram-positive bacterial membrane(44, 45), induced an immediate secondary structure transition of uperin 3.5 towards an α-helical conformation, with typical minima near 208 and 222 nm (Figure 2A). A similar phenomenon has been reported for other AMPs, which showed a random coil structure in solution, and a structural transition in the presence of membrane lipids (46).

The secondary structure of dry uperin 3.5 fibrils was evaluated using solid-state CD (ssCD) spectroscopy (47-51), previously shown to be highly applicable for characterization of aggregating proteins and peptides (48, 52-54). The ssCD spectrum measured for uperin 3.5 incubated in the absence of bacterial lipids indicated a β-rich conformation, with a typical minimum at 218 nm (Figure 2B). In contrast, uperin 3.5 fibrils incubated in the presence of DOPE:DOPG SUVs had a seemingly α-helical conformation (Figure 2B). While the fibril sample in the ssCD spectrum showed a deeper 222 nm minimum as compared to the 208 nm minimum, the sample in solution showed the opposite trend, with a deeper 208 nm minimum (Figure 2). The same trend was observed when analyzing a thin film of pre-formed PSMα3 fibrils (SI Appendix, Figure S4). The switch in the depth of the minima of fibrils versus soluble uperin 3.5 could be related to different secondary structure subpopulations, association between α-helices (55, 56), or other physicochemical properties. Adding DOPE:DOPG SUVs to the pre-formed β-rich uperin 3.5 fibrils, led to a transition towards an α-helical conformation (Figure 2C), providing further evidence of lipid-induced helicity, even after the fibrils were already formed.

The secondary structure of dry uperin 3.5 fibrils was further studied using attenuated total internal reflection Fourier-transform infrared (ATR-FTIR) spectroscopy, which was shown useful for characterization of fibrillar architectures in amyloid proteins and peptides (57-61).

The major peak in the amide-I' region of the IR absorption spectrum of uperin 3.5 fibrils was at 1616 cm^{-1}, indicative of the cross-β amyloid architecture (57-59), while the minor peak at 1652 cm^{-1}, was indicative of α-helices (60, 61) (Figure 2D), suggesting a mixed population with a predominant cross-β structure. Forming the fibrils in the presence of DOPE:DOPG SUVs resulted in a shifted IR spectrum, with a strong major peak at 1652 cm^{-1}, indicative of a majority of α-helices (Figure 2D). Additional minor peaks at 1616 and 1634 cm^{-1}, indicative of cross-β amyloids and regular β-sheets, respectively, suggested some remaining β-rich structures. The X-ray fiber diffraction of uperin 3.5 incubated in the absence of bacterial lipids, showed a cross-β signature (62), with orthogonal reflection arcs at 4.7 Å spacing (sharp) and at 7-11 Å (diffused) (SI Appendix, Figure S5). A fiber X-ray diffraction of uperin 3.5 fibrils grown in the presence of bacterial lipids showed strong reflections of the lipids, and the pattern of the protein was not adequately coherent for interpretations. Overall, these findings suggest a chameleon behavior of uperin 3.5, with transition from a random coil conformation in its soluble state to either a cross-β fibril conformation, formed in lipid-free solution, or to cross-α fibril structure, induced by the presence of bacterial membrane lipids.

Thermostability of uperin 3.5 fibrils might stem from their chameleon propensity

Uperin 3.5 fibrils were found to be thermostable, as observed in electron micrographs after a heat shock treatment of incubating the fibrils at 60°C for 10 min (Figure 3B). The ssCD spectrum of preformed uperin 3.5 fibrils indicated largely on β-rich species (Figure 2B&3A), while after the heat shock treatment a deeper minimum at 218 nm was observed, as compared with non-heat-shock treated fibrils of the same sample, indicating a larger population of β-rich species (Figure 3A). In comparison, *S. aureus* PSMα1 fibrils which bear a cross-β configuration (29), were also

thermostable, while the PSMα3 cross-α fibrils dissolved after the heat-shock treatment (SI Appendix, Figure S6), indicating on a fibril secondary-structure dependent thermostability.

Uperin 3.5 incubated in the presence of DOPE:DOPG SUVs showed massive fibril formation and thick fibrils around and on the SUVs (Figure 3B; SUVs incubated alone as control are shown in SI Appendix, Figure S7). The ssCD spectra indicated on a mixed population of species with a predominant α-helical conformation (Figure 3A). When subjected to a heat shock treatment, the uperin 3.5 fibrils formed in the presence of the SUVs remained stable, whereas the SUVs seemed to partially denature, as observed in the electron micrographs (Figure 3B), and the ssCD spectra indicated on a transition to a predominant β-rich architecture (Figure 3A). Overall, these findings demonstrate a heat-induced transition of uperin 3.5 fibrils to a predominantly β-rich conformation, which probably led to thermostability. This corresponds to the higher stability of the cross-β PSMα1 as compared to cross-α PSMα3 (SI Appendix, Figure S6), which are homologous sequences with fibrils of different secondary structures.

Uperin 3.5 fibrillation is involved in antibacterial activity

The antibacterial activity of uperin 3.5, examined using the disc (agar) diffusion test against four Gram-positive pathogens, demonstrated its more potent activity against *Micrococcus luteus* as compared to *Staphylococcus hominis*, *Staphylococcus epidermidis* and *Staphylococcus aureus* (Figure SI Appendix, S8), as previously reported (39). Using the standard broth dilution assay for quantification, a minimum inhibitory concentration (MIC) of freshly dissolved uperin 3.5 against *M. luteus*, defined as the lowest concentration that prevented bacterial growth for 24 h, was 2 µM (Table 2). Membrane surface topography analysis of *M. luteus* bacterial cells, visualized using scanning electron microscopy (SEM), indeed showed that overnight incubation with 2 µM

uperin 3.5 induced some membrane damage, while 6 μM uperin 3.5 induced severe morphological damage (Figure 4A). Higher-resolution TEM micrographs of 4 μM uperin 3.5 incubated for 24 h with *M. luteus* showed massive fibril formation around the bacterial cells, which led to cell death (Figure 4B). Uperin 3.5 incubated under the same conditions without the bacteria showed only scarce fibril formation (Figure 4B), suggesting that the presence of bacterial cells induced aggregation. A similar effect was observed in samples of uperin 3.5 with DOPE:DOPG SUVs, in which massive fibril formation was observed around the SUVs (Figure 3B).

In accordance with the above findings, light microscopy images showed that FITC-labelled uperin 3.5, which retained fibril-forming and antibacterial abilities (Table 2, and SI Appendix, Figure S9), accumulated on or inside rhodamine-labelled DOPE:DOPG SUVs (SI Appendix, Figure S10A) or *M. luteus* cells (SI Appendix, Figure S10B). The latter led to membrane permeation, followed by propidium iodide uptake, indicating cell death. Taken together, these findings demonstrate the bi-directional effects of uperin 3.5 and bacterial cells, namely the role of bacterial lipids in inducing cross-α fibrillation, and the role of cross-α fibrillation in antibacterial activity.

The heat shock-treated uperin 3.5 soluble peptide retained its antibacterial function, with a similar MIC against *M. luteus* cells, before as compared to after heat treatment (Table 2). In contrast, pre-formed uperin 3.5 fibrils (pre-incubated for 5 days) exhibited a heat-induced reduction in their antibacterial activity, with a MIC of 16 μM versus 4 μM following as compared to before heat treatment, respectively (Table 2). Of note, it is difficult to compare the activity of fresh and incubated samples due to the rapid aggregation rate and change in effective concentration. The heat-induced effect was compared using the same sample immediately pre- and post-heating, yet potential changes in fibril dynamics must also be considered when

analyzing the factors that affect activity. Moreover, since heat and the presence of lipids had opposite effects on the secondary structure of pre-formed uperin 3.5 fibrils (Figures 2&3A), it must be assumed that addition of uperin 3.5 to bacterial cells may partially reverse some of the heat-induced effects. Thus, the overall four-fold reduction in antibacterial activity of pre-formed fibrils after heating is likely the result of a combined effects of heat-induced secondary structure transition towards a β-rich conformation, altered dynamics between fibrils and monomers, changes in biophysical properties and effective concentration, and additional factors. Overall, the polymorphism within the same peptide sequence, and the mixture of populations, including different secondary structures and in/soluble states, present great challenges to structure-function-fibrillation relationships of functional fibrils in general. The presence of other components such as lipids and cells further affect the dynamic within species, increasing complexity and interpretations.

Discussion

Here, we revealed and characterized the functional cross-α fibril architecture formed by the eukaryotic uperin 3.5 AMP, and its chameleon secondary structure switch, putatively regulating activity. The helical fibril formation of uperin 3.5 was largely induced by, and formed on bacterial cells, where it consequently led to severe membrane damage and cell death (Figure 4 and SI Appendix, Figure S10). Of note, crystal structures of short helical AMPs are rather rare (63), nevertheless, quasiracemate crystal structures of frog AMP magainin 2 derivatives showed laterally stacked helices (64), similarly to the cross-α architecture. While correlations between amyloid formation and antibacterial activity have long been drawn (6-16, 20-26, 65), this work provided an atomic-level description for this link, involving a cross-α amyloid configuration. The departure of the secondary structure of the cross-α amyloid uperin 3.5 from the typical cross-β

configuration clarifies the connection between AMPs which are largely helical in nature, and amyloid formation. Interestingly, amyloids secreted from microbes, either during a pathogenic infection, or even by the gut microflora, have been implicated in the development of neurodegenerative and amyloid systemic disorders (66, 67). The overall connection between microbes, AMPs, the immune system, and neurodegenerative and systemic diseases requires more extensive studies.

In line with the reported polymorphism of cross-β amyloids (68), we observed polymorphism within the cross-α fibrils of uperin 3.5 and PSMα3. Both showed helical mated sheets of stacked amphipathic α-helices, which lay perpendicular to the fibril axis. PSMα3 contained parallel α-helices, while uperin 3.5 contained antiparallel helices within the sheets (Figure 1), further recapitulating the parallel and antiparallel β-sheet configurations. Similarly, an antiparallel cross-α crystal structure was shown in a designed synthetic peptide (35). Furthermore, the inter-helix and inter-sheet distances of uperin 3.5 were smaller than those in PSMα3, likely due to less bulky side chains, and due to the staggered sheets of uperin 3.5 (Figure 1). As amyloid polymorphism has been correlated with different toxicity level and prion disease strains (69, 70), the polymorphisms within cross-α structures may dictate toxicity levels, mechanisms of action, cell specificity, and fibril stability. While PSMα3 was stable as an α-helix in solution and in fibrils, uperin 3.5 helicity was dependent on the presence of lipids or other components. Moreover, while PSMα3 cross-α fibrils dissolved when subjected to heat shock, uperin 3.5 was thermostable (Figure 3B and SI Appendix, Figure S6), which is likely attributed to the heat-induced transition into cross-β fibrils (Figure 3A). In PSMα3, secondary structure changes were shown inducible via mutations (31) or truncations (29) which formed mixed α/β populations or exclusively β-rich structures (31). Of note, since we cannot determine the exact

composition of the uperin 3.5 samples, namely soluble vs insoluble species and mixture of different secondary structures, in real time of bacteria interaction, we can only suggest a trend based on our combined results, of a reduced activity of the β-rich polymorph.

Chameleon proteins that can adopt diverse secondary structures in response to external chemical or physical stimuli have been previously described (71-73), some induced by lipids or heat, (74-76), similar to what was observed here for uperin 3.5 fibrils (Figures 2 and 3). Martin, Carver and co-workers previously pointed on a potential chameleon propensity of uperin 3.5 (42), and discussed the role of helices as intermediates to aggregation (34, 42, 77, 78) along with the potential contribution of intermolecular helix–helix interactions in the formation of a fibrillation nuclei (42). A thermal-induced cross-α/cross-β transition was previously reported in a synthetic self-assembling heptapeptide, suggested to occur via an intermediate turn motif (34). In addition, a dipeptide protein-mimics, containing triazole linkages as peptide-bond surrogate, formed β-sheet rich structures in crystals, while heat-induced polymerization into a pseudoprotein revealed transition into helical sheets resembling the cross-α configuration (38). The seemingly relatively unstructured C-terminal region of uperin 3.5 (Figure 1), might be essential for the mechanism of cross-α/cross-β transition. An alternative suggestion for the transition mechanism of uperin 3.5 could stem from environmental effects on the equilibrium of mixed α/β species (Figure 2).

Taken together, we hypothesize that in the amphibian uperin 3.5, secreted on the skin of the toadlet (39), the chameleon secondary structure switch could be related to regulation of activity. Namely, uperin 3.5 monomers secreted on the amphibian skin have disordered structures, while the presence of bacterial cells induces helicity and cross-α formation, which putatively facilitates the antibacterial activity and eliminates the threat of infection. In the

absence of bacteria, uperin 3.5 assembles into inactive cross-β fibrils. This is somewhat similar to human amyloid toxicity which is debatably attributed to prefibrillar oligomeric conformations, which can contain α-helices(77), while the mature β-rich fibrils are considered less toxic (79). The β-rich uperin 3.5 can also serve as a reservoir (34, 80), presenting a means of storing a high local concentration of inactive uperin 3.5 on the amphibian skin, which can be switched back to helical conformation with the appearance of bacterial cells (as tested on mimetics, Figure 2C). We expect that additional studies will shed additional light on the underlying regulation.

The mechanism by which uperin 3.5 disrupts membranes is yet to be fully determined. Recently, we suggested a peptide-membrane co-aggregation model for PSMα3 toxicity against human cells (31). In this model, toxicity is not caused by a particular entity, such as monomers, oligomers, or fibrils. Rather, toxicity entails a dynamic process of peptide aggregation that is induced by, and involves, membrane lipids (31). Thus, both the presence of soluble species and the ability to fibrillate are critical determinants of toxicity. We suggest similar aggregation dynamics for uperin 3.5, in which cross-α fibrillation is both directly related to the presence of, and incorporates, membrane lipids (SI Appendix, Figure S10). However, we expect differences in the mechanisms of action of PSMα3 and uperin 3.5, due to the different properties of their fibrils and different sequences.

Altogether, the presented findings emphasize the structural complexity and the polymorphic nature of the amyloid fold, as shown in cross-α fibrils formed by prokaryotic and eukaryotic toxic peptides, namely the bacterial PSMα3 and the amphibian uperin 3.5. This extends the definition of amyloid structures, and of functional fibrils. The findings could lay the foundations for the design of novel synthetic AMPs with enhanced potency, stability, and

bioavailability, and with controllable storage and activities, to fight the growing threat of aggressive and resistant microbial infections.

Table 1 – Data collection and refinement statistics

Uperin 3.5 cross-α fibril	
PDB accession code	6GS3
Beamline	ESRF MASSIF-3
Date	April 19, 2017
Data collection	
Space group	P 1 2_1 1
Cell dimensions	
a, *b*, *c* (Å)	19.70, 28.44, 20.32
α, β, γ (°)	90.00, 106.95, 90.0
Wavelength (Å)	0.968
Resolution (Å)	19.47-1.45 (1.49-1.45)
R-factor observed (%)	8.5 (60.1)
[a] R_{meas} (%)	8.9 (64.8)
$I / \sigma I$	15.7 (2.7)
Completeness (%)	97.0 (94.7)
Redundancy	10.6 (7.6)
[b] $CC_{1/2}$ (%)	99.9 (90.8)
Refinement	
Resolution (Å)	19.44-1.45 (1.49-1.45)
Completeness (%)	97.2 (94.7)
[c] No. reflections	3398 (238)
[d] R_{work} (%)	18.5 (24.4)
R_{free} (%)	22.9 (28.0)
No. atoms	275
Protein	254
Ligand/ion	5
Water	16
B-factors	
Protein	15.1 (Chain A) 12.7 (Chain B)
Ligand/ion	41.4 (K^+) 19.3 (SCN^-)

Water	21.6
R.m.s. deviations	
Bond lengths (Å)	0.016
Bond angles (°)	1.783
Clash score(81)	0
Molprobity score(81)	0.5
Molprobity percentile(81)	100th percentile
Number of crystals used for scaling	1

Values in parentheses are for highest-resolution shell.

[a] R-meas is a redundancy-independent R-factor defined in (82).

(b) $CC_{1/2}$ is percentage of correlation between intensities from random half-datasets (83).

(c) Number of reflections corresponds to the working set.

(d) Rwork corresponds to working set.

Table 2 - Uperin 3.5 antibacterial activity against *Micrococcus luteus*

Uperin 3.5	**MIC (µM)**	**MIC (µM)** **after 60°C treatment**
Freshly dissolved	2	2
5-days incubated	4	16
Freshly dissolved FITC-labeled	8	-

Figure 1. The cross-α amyloid fibril architectures of uperin 3.5 versus PSMα3

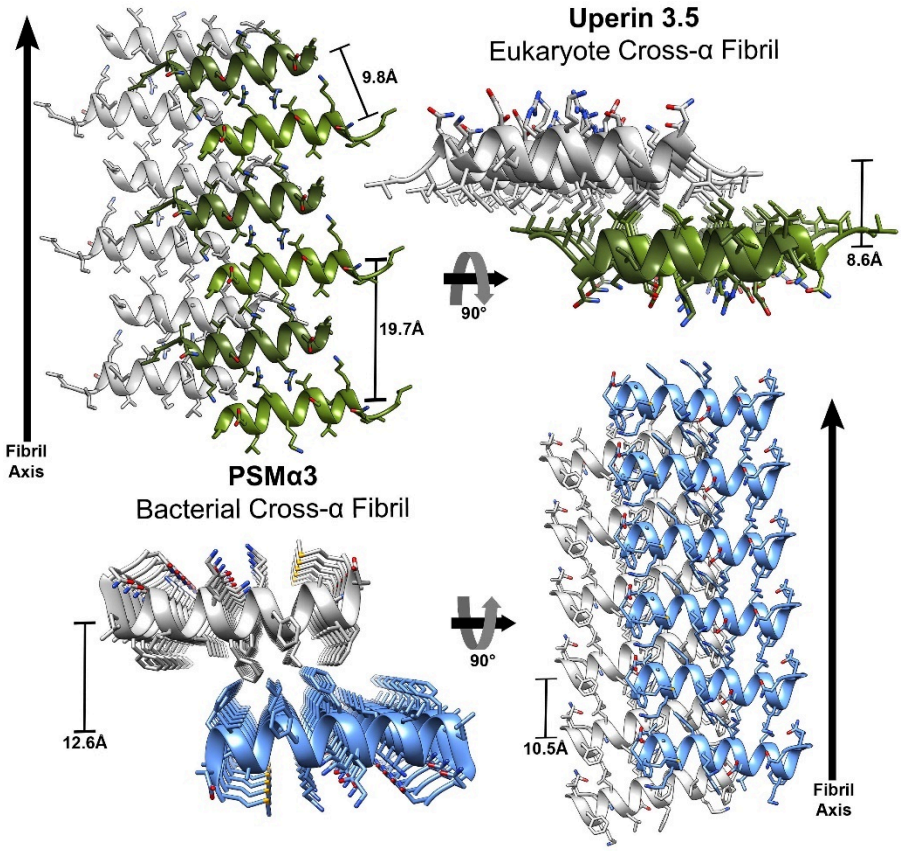

The crystal structures of uperin 3.5 (PDB ID: 6GS3) (green and grey ribbons) and PSMα3 (PDB ID: 5I55) (30) (blue and grey ribbons) cross-α fibrils are shown in two orientations: down and along the fibril axis. Two mated helical sheets are displayed in each panel, with six layers of laterally stacked α-helices depicted in each sheet (fibrils are likely composed of thousands of layers). The α-helical sheets interact via their hydrophobic face to create a tight interface. In contrast to the parallel orientation of the helices along the sheets of PSMα3, the helices in uperin 3.5, colored in different shades of green for clarity, take on an antiparallel orientation. The distances between helices along the sheets and between sheets are shown in each panel. In both panels, side chains are shown as sticks with heteroatoms colored by atom type (nitrogen in blue, oxygen in red and sulfur in yellow).

Figure 2. Bacterial lipids induce uperin 3.5 secondary structure transition into α-helical species in soluble and fibrillar states

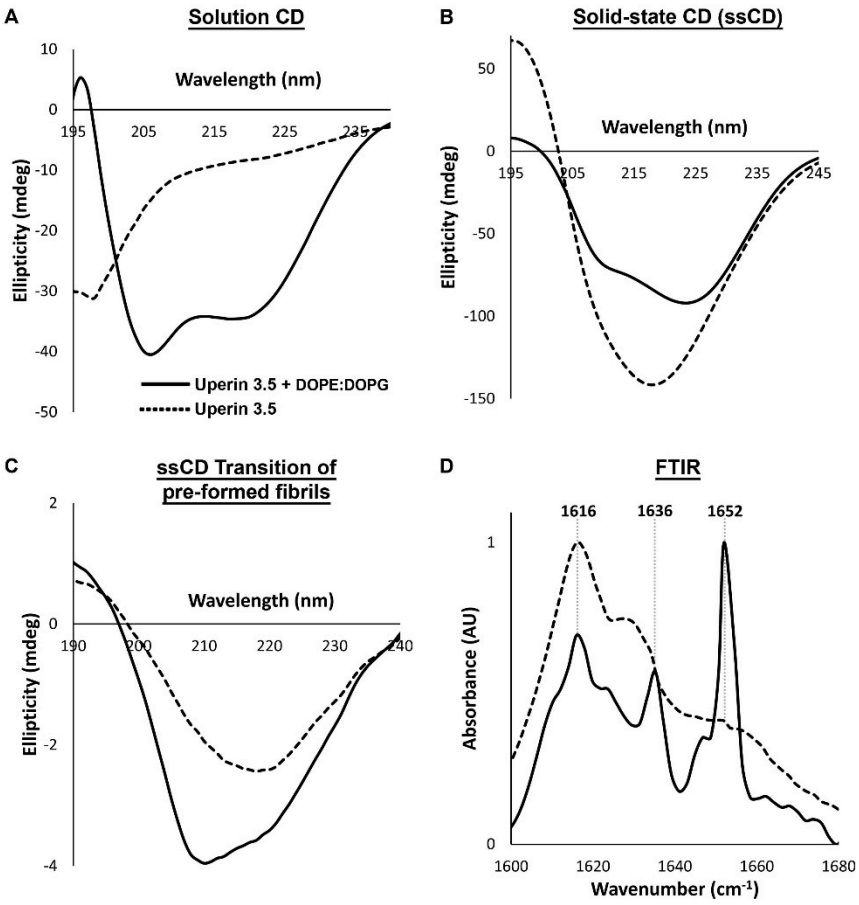

(**a**) Solution CD spectra of uperin 3.5, indicating a random coil conformation (dashed curve). Upon addition of DOPE:DOPG SUVs, the uperin 3.5 structure immediately transitioned and stabilized in a dominant α-helical conformation (solid curve). (**b**) Solid-state CD (ssCD) spectra of uperin 3.5 fibrils, indicating the formation of β-rich fibrils (dashed curve). When incubated with DOPE:DOPG SUVs, the fibrils took on a α-helical conformation (solid curve). The ssCD spectrum of the cross-α fibrils of PSMα3 are shown in SI Appendix, Figure S4 for comparison. (**c**) ssCD spectra of an uperin 3.5 thin-film, indicating the formation of β-rich fibrils (dashed curve). The addition of DOPE:DOPG SUVs solution on to the thin film of pre-formed β-rich fibrils resulted in a secondary structure transition towards the α-helical conformation (solid curve). (**d**) ATR-FTIR spectra of the amide I' region of uperin 3.5 fibrils (dashed curve) showed a major peak at 1616

cm^{-1}, indicative of cross-β amyloids (57-59). Uperin 3.5 fibrils formed in the presence of DOPE:DOPG SUVs (solid curve) demonstrated a major peak at 1652 cm^{-1}, indicative of α-helices (60, 61) and a minor peak at 1616 cm^{-1}, indicative of residual β-rich fibrils. The dotted grey lines indicate wavenumbers of 1616, 1634 and 1652 cm^{-1}. In all experiments (a-d), the signal of buffer only or DOPE:DOPG SUVs solution was negligible and subtracted from each measured sample.

Figure 3. Thermal stability and the effect of heat on the secondary structure of uperin 3.5 fibrils

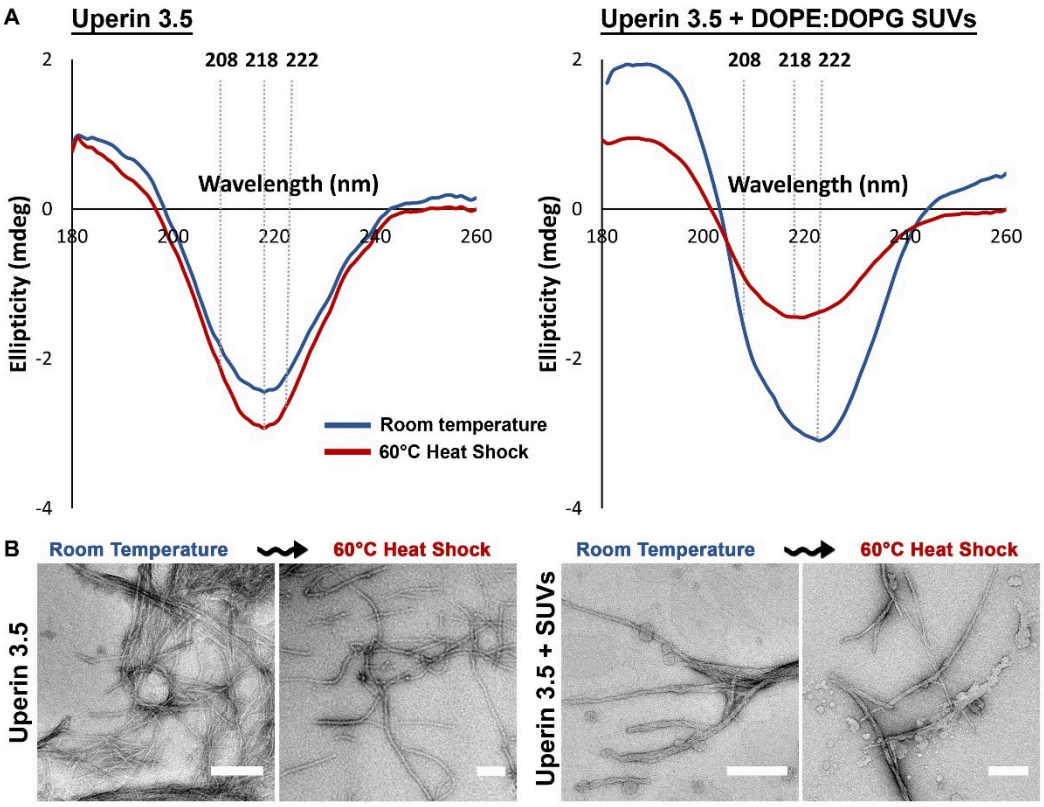

(**a**) Solid-state CD (ssCD) spectra showing the effect of heating on the secondary structure of pre-formed thin films of uperin 3.5 fibrils formed alone or in the presence of DOPE:DOPG SUVs. Left panel: uperin 3.5 incubated alone showed a predominant β-rich fibril conformation before and after a 10 min, 60°C heat shock treatment (blue and red curves, respectively). Right panel: uperin 3.5 fibrils formed in the presence of DOPE:DOPG SUVs showed predominant α-helical fibril conformation (blue curve), while after a 10 min, 60°C heat-shock treatment, it showed a secondary structure transition towards a β-rich conformation (red curve). The dotted grey lines indicate wavelengths of 208 nm, 218 nm, and 222 nm. The same sample was tested following temperature change in both assays. (**b**) TEM micrographs of 1 mM uperin 3.5 incubated for 2 days at room-temperature alone, or in the presence of DOPE:DOPG SUVs, showing thermostable fibrils. Scale bars represent 300 nm. The same sample was tested following

temperature change in both assays. TEM micrographs of DOPE:DOPG SUVs incubated alone as control are shown in SI Appendix, Figure S7.

Figure 4. Electron micrographs of uperin 3.5 fibrils formed on bacterial cells and of uperin 3.5-induced membrane damage

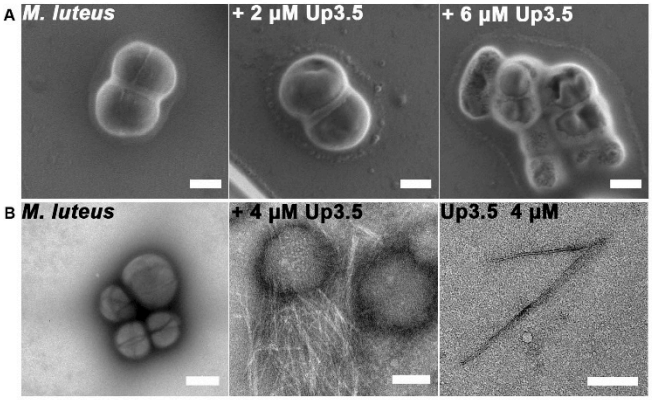

(**a**) Scanning electron microscopy (SEM) images showing *M. luteus* cells incubated for 24 h in the absence (left) or presence of uperin 3.5 at 2 µM (middle) and 6 µM (right), and resultant membrane dents. Scale bars represent 500 nm for all images. (**b**) Transmission electron micrographs of *M. luteus* cells incubated in the absence (left) or presence (middle) of 4 µM uperin 3.5 for 24 h, showing massive fibril formation around bacterial cells (middle panel). Scarce fibril formation is shown upon incubation without cells (right panel). Scale bars represent 1 µm for *M. luteus* (left), and 200 nm for *M. luteus* incubated with uperin 3.5 (middle) and for uperin 3.5 incubated alone (right).

Materials and Methods

A full methodological description is provided in the SI Appendix.

Peptides: Uperin 3.5 peptide (Uniprot accession code: P82042) of the sequence GVGDLIRKAVSVIKNIV-NH2, PSMα1 (Uniprot accession code: H9BRQ5) of the sequence MGIIAGIIKVIKSLIEQFTGK and PSMα3 (Uniprot accession code: H9BRQ7) of the sequence MEFVAKLFKFFKDLLGKFLVNN, were all custom synthesis at >98% purity. Peptide pre-treatment, and preparation of the small unilamellar vesicle (SUV) are described in the SI Appendix.

Fibrillation assays of uperin 3.5, with and without lipids, and/or bacterial cells, were conducted using Thioflavin T (ThT) fluorescence fibrillation kinetics assay, and transmission electron microscopy (TEM). Thermostability assays were performed using TEM.

Crystallization conditions, structure determination and refinement: Non-pretreated uperin 3.5 peptide synthesized with free (unmodified) termini, was dissolved in ultra-pure water, to 10 mM, followed by a 10 min sonication in a bath sonicator, at room temperature. All crystals were grown, at 20 °C, via hanging-drop vapor diffusion. The drop was a mixture of peptide in reservoir solution (0.1 M KSCN, 0.1 M MES pH 6.03 and 20 %v/v Jeff 600). Crystals were flash-frozen with cryoprotection of 20 % ethylene-glycol and stored in liquid nitrogen prior to data collection. X-ray diffraction data were collected at 100 K, at the micro-focus beamline Massif-III (ID30a-III) of the European Synchrotron Radiation Facility (ESRF) in Grenoble, France; wavelength of data collection was 0.9677 Å. Data indexation, integration and scaling were performed using XDS/XSCALE (84). Phases were obtained using ARCIMBOLDO_LITE (85), Model building was done using Coot (86). Crystallographic refinements were performed with Refmac5

(87), and illustrated with Chimera (88). Crystallographic parameters are listed in Table 1. Calculations of structural properties are described in the SI appendix.

Solution circular dichroism (CD) spectroscopy: Pre-treated uperin 3.5 was dissolved to 10 mM in ultra-pure water and diluted to 1 mM in 20 mM potassium phosphate buffer and 100 mM NaCl, pH 7.3. Uperin 3.5 was diluted in the CD cuvette to a final concentration of 0.2 mM, in the presence or absence of 0.6 mM SUVs. For Solid-state circular dichroism (ssCD) spectroscopy, uperin 3.5 (5 mg/ml) dissolved in ultra-pure water and uperin 3.5 (1.8 mg/ml) mixed with DOPE:DOPG SUVs solution at a 1:3 peptide:lipid molar ratio were incubated at 37 ℃, with 300 rpm shaking, for 2 days. PSMα3 (5 mg/ml) dissolved in ultra-pure water was incubated at 37 ℃, with 300 rpm shaking, for 2 days. Fibrillated samples were centrifuged at 10,000 g for 5 min and re-suspended in ultra-pure water. For the Thermostability assays uperin 3.5 pre-treated samples were dissolved in ultra-pure water to 1mM (1.8 mg/ml), mixed with DOPE:DOPG SUVs at a 1:3 peptide:lipid ratio and incubated for 5 days at room temperature. The ssCD spectra of each sample was measured at room temperature, and again after a 10 min, 60 ℃ heat-shock, while still being placed as a thin-film on the disc.

Attenuated total internal reflections Fourier transform infrared (ATR-FTIR) spectroscopy: Uperin 3.5 was dissolved to 1 mg/ml in 5 mM hydrochloric acid (HCl) and sonicated in a bath sonicator for 5 min, at room temperature. Immediately prior to measurements, the dry peptide was dissolved either in D_2O, with or without SUVs, to a final concentration of 20 mg/ml, with a 1:1 peptide:lipid molar ratio.

Antibacterial assays: *Micrococcus luteus* (an environmental isolate) was a kind gift from Prof. Charles Greenblatt from the Hebrew University in Jerusalem, Israel. *Staphylococcus hominis* (ATTC 27844), *Staphylococcus aureus* (ATCC 29213) and *Staphylococcus epidermidis* (ATCC

12228) were purchased. *M. luteus* was cultured in Luria-Bertani (LB) medium at 30℃, with 250 rpm shaking, overnight. *S. aureus*, *S. hominis* and *S. epidermidis* were cultured in brain-heart infusion (BHI) medium, at 37 ℃, with 250 rpm shaking, overnight. Disc (agar) diffusion test, determination of the minimal inhibitory concentration (MIC), scanning electron microscopy (SEM). and fluorescence microscopy are described in the SI appendix.

Acknowledgments

We wish to thank Sunny Singh for initiating fibrillation experiments and crystallization. We acknowledge guidance and technical support provided by Yael Pazy-Benhar and Dikla Hiya at the Technion Center for Structural Biology (TCSB). We acknowledge support from Yaron Kauffmann from the MIKA electron microscopy center of the Department of Material Science & Engineering at the Technion, Na'ama Koifman from the Russell Berrie Electron Microscopy Center of Soft Matter at the Technion, Nitsan Dahan and Yael Lupo-Haber from the Life Science and Engineering Infrastructure Center, Rachel Edrey from the Chemical and Surface Analysis Laboratory, at the Department of Chemistry, all at the Technion, Israel. This research was supported by Israel Science Foundation (grant no. 560/16), Israel Ministry of Science, Technology & Space (grant no. 78567), U.S.-Israel Binational Science Foundation (BSF) (grant no. 2017280), BioStruct-X, funded by FP7, and the iNEXT consortium of Instruct-ERIC. The synchrotron MX data collection experiments were performed at beamlines ID29, ID23-EH2 and ID30A-3 / MASSIF-3 at the European Synchrotron Radiation Facility (ESRF), Grenoble, France, and at beamline P14, operated by EMBL Hamburg at the PETRA III storage ring (DESY, Hamburg, Germany). We are grateful to the teams at ESRF and EMBL Hamburg.

Competing interests

The authors declare no competing interests.

References

1. K. A. Brogden, Antimicrobial peptides: pore formers or metabolic inhibitors in bacteria? *Nature Reviews Microbiology* **3**, 238-250 (2005).
2. M. N. Melo, R. Ferre, M. A. R. B. Castanho, Antimicrobial peptides: linking partition, activity and high membrane-bound concentrations. *Nature Reviews Microbiology* **7**, 245-250 (2009).
3. L.-J. Zhang, R. L. Gallo, Antimicrobial peptides. *Current Biology* **26**, R14-R19 (2016).
4. M. Mahlapuu, J. Håkansson, L. Ringstad, C. Björn, Antimicrobial Peptides: An Emerging Category of Therapeutic Agents. *Frontiers in cellular and infection microbiology* **6** (2016).
5. Z. Ye *et al.*, Self-assembly dynamics and antimicrobial activity of all l- and d-amino acid enantiomers of a designer peptide. *Nanoscale* **11**, 266-275 (2018).
6. B. L. Kagan *et al.*, Antimicrobial properties of amyloid peptides. *Mol Pharm* **9**, 708-717 (2012).
7. H. Zhao *et al.*, Interaction of the antimicrobial peptide pheromone Plantaricin A with model membranes: implications for a novel mechanism of action. *Biochim Biophys Acta* **1758**, 1461-1474 (2006).
8. C. Auvynet *et al.*, Structural requirements for antimicrobial versus chemoattractant activities for dermaseptin S9. *The FEBS journal* **275**, 4134-4151 (2008).
9. Y. A. Domanov, P. K. Kinnunen, Antimicrobial peptides temporins B and L induce formation of tubular lipid protrusions from supported phospholipid bilayers. *Biophysical journal* **91**, 4427-4439 (2006).
10. L. Caillon, J. A. Killian, O. Lequin, L. Khemtemourian, Biophysical investigation of the membrane-disrupting mechanism of the antimicrobial and amyloid-like peptide dermaseptin S9. *PLoS One* **8**, e75528 (2013).
11. P. Chairatana, E. M. Nolan, Human alpha-Defensin 6: A Small Peptide That Self-Assembles and Protects the Host by Entangling Microbes. *Accounts of chemical research* **50**, 960-967 (2017).
12. X. Tian, F. Sun, X. R. Zhou, S. Z. Luo, L. Chen, Role of peptide self-assembly in antimicrobial peptides. *J Pept Sci* **21**, 530-539 (2015).
13. H. Chu *et al.*, Human alpha-defensin 6 promotes mucosal innate immunity through self-assembled peptide nanonets. *Science* **337**, 477-481 (2012).
14. L. Schnaider *et al.*, "Self-assembling dipeptide antibacterial nanostructures with membrane disrupting activity" in Nat Commun. (2017), vol. 8.
15. M. Zhang, J. Zhao, J. Zheng, Molecular understanding of a potential functional link between antimicrobial and amyloid peptides. *Soft Matter* **10**, 7425-7451 (2014).
16. H. Zhao *et al.*, Binding of endostatin to phosphatidylserine-containing membranes and formation of amyloid-like fibers. *Biochemistry* **44**, 2857-2863 (2005).
17. H. Jang *et al.*, Antimicrobial protegrin-1 forms amyloid-like fibrils with rapid kinetics suggesting a functional link. *Biophys J* **100**, 1775-1783 (2011).
18. C. M. Dobson, Protein misfolding, evolution and disease. *Trends Biochem. Sci.* **24**, 329-332 (1999).
19. D. Eisenberg, M. Jucker, The amyloid state of proteins in human diseases. *Cell* **148**, 1188-1203 (2012).

20. S. J. Soscia *et al.*, The Alzheimer's disease-associated amyloid beta-protein is an antimicrobial peptide. *PLoS One* **5**, e9505 (2010).
21. D. K. Kumar *et al.*, Amyloid-beta peptide protects against microbial infection in mouse and worm models of Alzheimer's disease. *Science translational medicine* **8**, 340ra372 (2016).
22. S. C. Park *et al.*, Functional characterization of alpha-synuclein protein with antimicrobial activity. *Biochem Biophys Res Commun* **478**, 924-928 (2016).
23. Y. Hirakura, I. Carreras, J. D. Sipe, B. L. Kagan, Channel formation by serum amyloid A: a potential mechanism for amyloid pathogenesis and host defense. *Amyloid* **9**, 13-23 (2002).
24. N. B. Last, A. D. Miranker, Common mechanism unites membrane poration by amyloid and antimicrobial peptides. *Proc Natl Acad Sci U S A* **110**, 6382-6387 (2013).
25. K. Bourgade *et al.*, beta-Amyloid peptides display protective activity against the human Alzheimer's disease-associated herpes simplex virus-1. *Biogerontology* **16**, 85-98 (2015).
26. M. Pasupuleti *et al.*, "Antimicrobial Activity of Human Prion Protein Is Mediated by Its N-Terminal Region" in PLoS One. (2009), vol. 4.
27. R. Wang *et al.*, Identification of novel cytolytic peptides as key virulence determinants for community-associated MRSA. *Nat Med* **13**, 1510-1514 (2007).
28. K. Schwartz, A. K. Syed, R. E. Stephenson, A. H. Rickard, B. R. Boles, Functional amyloids composed of phenol soluble modulins stabilize Staphylococcus aureus biofilms. *PLoS Pathog* **8**, e1002744 (2012).
29. N. Salinas, J. P. Colletier, A. Moshe, M. Landau, Extreme amyloid polymorphism in Staphylococcus aureus virulent PSMalpha peptides. *Nat Commun* **9**, 3512 (2018).
30. E. Tayeb-Fligelman *et al.*, The cytotoxic Staphylococcus aureus PSMalpha3 reveals a cross-alpha amyloid-like fibril. *Science* **355**, 831-833 (2017).
31. E. Tayeb-Fligelman, N. Salinas, O. Tabachnikov, M. Landau, Staphylococcus aureus PSMalpha3 Cross-alpha Fibril Polymorphism and Determinants of Cytotoxicity. *Structure* **28**, 301-313.e306 (2020).
32. G. Y. Cheung, A. C. Duong, M. Otto, Direct and synergistic hemolysis caused by Staphylococcus phenol-soluble modulins: implications for diagnosis and pathogenesis. *Microbes and infection / Institut Pasteur* **14**, 380-386 (2012).
33. E. Hellstrand, A. Nowacka, D. Topgaard, S. Linse, E. Sparr, Membrane lipid co-aggregation with α-synuclein fibrils. *PLoS One* **8**, e77235 (2013).
34. S. Mondal *et al.*, Transition of Metastable Cross-α Crystals into Cross-β Fibrils by β-Turn Flipping. *Journal of the American Chemical Society* **141**, 363-369 (2019).
35. S.-Q. Zhang *et al.*, Designed peptides that assemble into cross-α amyloid-like structures. *Nature Chemical Biology* **14**, 870-875 (2018).
36. S. Bera *et al.*, Rigid helical-like assemblies from a self-aggregating tripeptide. *Nature Materials* **18**, 503-509 (2019).
37. Z. Yao *et al.*, Use of a Stereochemical Strategy To Probe the Mechanism of Phenol-Soluble Modulin α3 Toxicity. *J Am Chem Soc* **141**, 7660-7664 (2019).

38. K. Hema, K. M. Sureshan, β-Sheet to Helical-Sheet Evolution Induced by Topochemical Polymerization: Cross-α-Amyloid-like Packing in a Pseudoprotein with Gly-Phe-Gly Repeats. *Angewandte Chemie International Edition* **59**, 8854-8859 (2020).
39. A. Bradford, J. Bowie, M. Tyler, J. Wallace, New Antibiotic Uperin Peptides From the Dorsal Glands of the Australian Toadlet <I>Uperoleia mjobergii</I>. *Australian Journal of Chemistry* **49**, 1325-1331 (1996).
40. A. N. Calabrese *et al.*, The Amyloid Fibril-Forming Properties of the Amphibian Antimicrobial Peptide Uperin 3.5. *Chembiochem* **17**, 239-246 (2016).
41. L. L. Martin *et al.*, Amyloid aggregation and membrane activity of the antimicrobial peptide uperin 3.5. *Peptide Science* **110**, e24052 (2018).
42. T. John *et al.*, The Kinetics of Amyloid Fibrillar Aggregation of Uperin 3.5 Is Directed by the Peptide's Secondary Structure. *Biochemistry* **58**, 3656-3668 (2019).
43. T. John *et al.*, Adsorption of Amyloidogenic Peptides to Functionalized Surfaces Is Biased by Charge and Hydrophilicity. *Langmuir : the ACS journal of surfaces and colloids* **35**, 14522-14531 (2019).
44. C. Sohlenkamp, O. Geiger, Bacterial membrane lipids: diversity in structures and pathways. *FEMS microbiology reviews* **40**, 133-159 (2016).
45. R. F. Epand, P. B. Savage, R. M. Epand, Bacterial lipid composition and the antimicrobial efficacy of cationic steroid compounds (Ceragenins). *Biochimica et Biophysica Acta (BBA) - Biomembranes* **1768**, 2500-2509 (2007).
46. L. M. Yin, M. A. Edwards, J. Li, C. M. Yip, C. M. Deber, Roles of hydrophobicity and charge distribution of cationic antimicrobial peptides in peptide-membrane interactions. *Journal of Biological Chemistry* **287**, 7738-7745 (2012).
47. L. Stevens, R. Townend, S. N. Timasheff, G. D. Fasman, J. Potter, The circular dichroism of polypeptide films. *Biochemistry* **7**, 3717-3720 (1968).
48. J. Safar, P. P. Roller, D. C. Gajdusek, C. J. Gibbs, Thermal stability and conformational transitions of scrapie amyloid (prion) protein correlate with infectivity. **2**, 2206-2216 (1993).
49. F. Formaggio, M. Crisma, C. Toniolo, J. Kamphuis, Solid-state CD and peptide helical screw sense. *Biopolymers* **38**, 301-304 (1996).
50. P. McPhie, Circular Dichroism Studies on Proteins in Films and in Solution: Estimation of Secondary Structure by g-Factor Analysis. *Analytical biochemistry* **293**, 109-119 (2001).
51. H.-Y. Hu, Q. Li, H.-C. Cheng, H.-N. Du, β-Sheet structure formation of proteins in solid state as revealed by circular dichroism spectroscopy. *Biopolymers* **62**, 15-21 (2001).
52. P. McPhie, CD studies on films of amyloid proteins and polypeptides: Quantitative g-factor analysis indicates a common folding motif. *Biopolymers* **75**, 140-147 (2004).
53. T. Harada, R. Kuroda, CD measurements of beta-amyloid (1-40) and (1-42) in the condensed phase. *Biopolymers* **95**, 127-134 (2011).
54. H. Y. Hu, L. L. Jiang, J. Y. Hong, Study of Protein Amyloid-Like Aggregates by Solid-State Circular Dichroism Spectroscopy. *Current protein & peptide science* **18**, 100-103 (2017).

55. T. M. Cooper, R. W. Woody, The effect of conformation on the CD of interacting helices: a theoretical study of tropomyosin. *Biopolymers* **30**, 657-676 (1990).
56. N. E. Zhou, C. M. Kay, R. S. Hodges, Synthetic model proteins. Positional effects of interchain hydrophobic interactions on stability of two-stranded alpha-helical coiled-coils. *J Biol Chem* **267**, 2664-2670 (1992).
57. S. D. Moran, M. T. Zanni, How to Get Insight into Amyloid Structure and Formation from Infrared Spectroscopy. *The Journal of Physical Chemistry Letters* **5**, 1984-1993 (2014).
58. R. Sarroukh, E. Goormaghtigh, J. M. Ruysschaert, V. Raussens, ATR-FTIR: a "rejuvenated" tool to investigate amyloid proteins. *Biochim Biophys Acta* **1828**, 2328-2338 (2013).
59. G. Zandomeneghi, M. R. Krebs, M. G. McCammon, M. Fandrich, FTIR reveals structural differences between native beta-sheet proteins and amyloid fibrils. *Protein Sci* **13**, 3314-3321 (2004).
60. P. I. Haris, D. Chapman, The conformational analysis of peptides using Fourier transform IR spectroscopy. *Biopolymers* **37**, 251-263 (1995).
61. T. Miyazawa, E. R. Blout, The Infrared Spectra of Polypeptides in Various Conformations: Amide I and II Bands1. *Journal of the American Chemical Society* **83**, 712-719 (1961).
62. M. Sunde *et al.*, Common core structure of amyloid fibrils by synchrotron X-ray diffraction. *J Mol Biol* **273**, 729-739 (1997).
63. S. Baeriswyl *et al.*, X-ray Crystal Structures of Short Antimicrobial Peptides as Pseudomonas aeruginosa Lectin B Complexes. *ACS chemical biology* **14**, 758-766 (2019).
64. Z. Hayouka *et al.*, Quasiracemate Crystal Structures of Magainin 2 Derivatives Support the Functional Significance of the Phenylalanine Zipper Motif. *J Am Chem Soc* **137**, 11884-11887 (2015).
65. H. Jang *et al.*, "Antimicrobial Protegrin-1 Forms Amyloid-Like Fibrils with Rapid Kinetics Suggesting a Functional Link" in Biophys J. (2011), vol. 100, pp. 1775-1783.
66. M. Sochocka *et al.*, The Gut Microbiome Alterations and Inflammation-Driven Pathogenesis of Alzheimer's Disease-a Critical Review. *Mol Neurobiol* 10.1007/ s12035-018-1188-4 (2018).
67. G. Sharon, T. R. Sampson, D. H. Geschwind, S. K. Mazmanian, The Central Nervous System and the Gut Microbiome. *Cell* **167**, 915-932 (2016).
68. J.-P. Colletier *et al.*, Molecular basis for amyloid-beta polymorphism. *Proceedings of the National Academy of Sciences of the United States of America* **108**, 16938-16943 (2011).
69. U. Ghosh, W. M. Yau, R. Tycko, Coexisting order and disorder within a common 40-residue amyloid-beta fibril structure in Alzheimer's disease brain tissue. *Chem Commun (Camb)* **54**, 5070-5073 (2018).
70. W. Close *et al.*, Physical basis of amyloid fibril polymorphism. *Nat Commun* **9**, 699 (2018).

71. W. Kabsch, C. Sander, On the use of sequence homologies to predict protein structure: identical pentapeptides can have completely different conformations. *Proc Natl Acad Sci U S A* **81**, 1075-1078 (1984).
72. D. L. Minor, Jr., P. S. Kim, Context is a major determinant of beta-sheet propensity. *Nature* **371**, 264-267 (1994).
73. B. Kim *et al.*, Aggregation of Chameleon Peptides: Implications of α-Helicity in Fibril Formation. *J Phys Chem B* **120**, 5874-5883 (2016).
74. E. K. Roberts *et al.*, Post-assembly alpha-helix to beta-sheet structural transformation within SAF-p1/p2a peptide nanofibers. *Soft Matter* **14**, 8986-8996 (2018).
75. M. Magzoub, L. E. Eriksson, A. Graslund, Conformational states of the cell-penetrating peptide penetratin when interacting with phospholipid vesicles: effects of surface charge and peptide concentration. *Biochim Biophys Acta* **1563**, 53-63 (2002).
76. S. Zhang, A. Rich, Direct conversion of an oligopeptide from a beta-sheet to an alpha-helix: a model for amyloid formation. *Proc Natl Acad Sci U S A* **94**, 23-28 (1997).
77. D. Ghosh *et al.*, Structure based aggregation studies reveal the presence of helix-rich intermediate during alpha-Synuclein aggregation. *Sci Rep* **5**, 9228 (2015).
78. V. L. Anderson, T. F. Ramlall, C. C. Rospigliosi, W. W. Webb, D. Eliezer, Identification of a helical intermediate in trifluoroethanol-induced alpha-synuclein aggregation. *Proc Natl Acad Sci U S A* **107**, 18850-18855 (2010).
79. M. Stefani, Structural features and cytotoxicity of amyloid oligomers: implications in Alzheimer's disease and other diseases with amyloid deposits. *Progress in neurobiology* **99**, 226-245 (2012).
80. S. K. Maji *et al.*, Functional amyloids as natural storage of peptide hormones in pituitary secretory granules. *Science* **325**, 328-332 (2009).
81. V. B. Chen *et al.*, MolProbity: all-atom structure validation for macromolecular crystallography. *Acta Crystallogr D Biol Crystallogr* **66**, 12-21 (2010).
82. K. Diederichs, P. A. Karplus, Improved R-factors for diffraction data analysis in macromolecular crystallography. *Nature structural biology* **4**, 269-275 (1997).
83. P. A. Karplus, K. Diederichs, Linking crystallographic model and data quality. *Science* **336**, 1030-1033 (2012).
84. W. Kabsch, XDS. *Acta Crystallogr D Biol Crystallogr* **66**, 125-132 (2010).
85. M. Sammito *et al.*, ARCIMBOLDO_LITE: single-workstation implementation and use. *Acta Crystallographica Section D* **71**, 1921-1930 (2015).
86. P. Emsley, B. Lohkamp, W. G. Scott, K. Cowtan, Features and development of Coot. *Acta Crystallogr D Biol Crystallogr* **66**, 486-501 (2010).
87. G. N. Murshudov, A. A. Vagin, E. J. Dodson, Refinement of macromolecular structures by the maximum-likelihood method. *Acta Crystallogr. D Biol. Crystallogr.* **53**, 240-255 (1997).
88. E. F. Pettersen *et al.*, UCSF Chimera--a visualization system for exploratory research and analysis. *Journal of computational chemistry* **25**, 1605-1612 (2004).